Solid Freeform Fabrication 2022: Proceedings of the 33rd Annual International Solid Freeform Fabrication Symposium – An Additive Manufacturing Conference
Reviewed Paper

Design and Additive Manufacturing of Bio-Inspired Copper Heat Sinks for Microelectronics Cooling

Jordan Yaple[1], Cameron Noe[1], Abdulmajeed Alenezi [2], Patrick Phelan[2], Dhruv Bhate[1]

[1]3DX Research Group, Arizona State University, Mesa, AZ 85121
[2]School of Matter, Energy and Transport Engineering, Arizona State University, Tempe, AZ

Abstract

The heat sink is a key component in thermal management of microelectronics and is traditionally designed with arrays of pins or fins. In this work, a bio-inspired approach to designing heat sinks was evaluated. A process was first developed on a 100W Laser Powder Bed Fusion (LPBF) system for the copper alloy CuNi2SiCr, which was found to have a tenfold deficit in thermal conductivity relative to commercially pure Copper. This process was then used to fabricate four heat sinks: two replicates of commercial heat sink designs, and two leveraging bio-inspired design approaches with the aim of increasing the available surface area per unit volume. The four designs were tested on a microelectronics package placed on a hot plate and their performance compared against commercially available heat sinks. The results demonstrated that despite their poor thermal conductivity, the bio-inspired heat sinks had equivalent performance to the commercial heat sinks.

Introduction

Of all the alloys developed for the Laser Powder Bed Fusion (LPBF) process, copper alloys have emerged only recently as a viable metal to fabricate parts from. LPBF of copper has had several challenges associated with it, stemming primarily from its low absorbance in comparison of incident laser energy relative to other well-qualified LPBF alloys [1]. In addition to processability challenges, risk of damage to optical components [2], oxidization of copper [3], relatively low density [4] have also been identified as potential issues with the LPBF of copper. Once a sufficiently dense part is created, there are limitations in an application context from excessive surface roughness [3], [5]. Nonetheless, prior work has demonstrated the feasibility of fabricating components using LPBF of copper alloy [6], and this forms the basis for the work here, which is an exploration of the use of LPBF and a specific copper alloy (CuNi2SiCr) for the fabrication of heat sinks for microelectronics cooling, previously published as a Master's thesis [7]. The three main objectives for this work were:

1. Development of a working process for LPBF for CuNi2SiCr with an as-printed density at least exceeding 94%. This criterion was based on prior literature where densities in excess of 94% were shown to be feasible.
2. Manufacture and compare the cooling effect of commercially available (COM) heat sinks against nominally identical additively manufactured (AM) heat sinks.
3. Design, fabrication, and evaluation of bio-inspired heat sinks.

The flow of this paper is as follows: the designs are first discussed, including the motivation for the bio-inspired designs, followed by the manufacturing aspects of this work, including the process development for the copper alloy, followed by the fabrication of the heat sinks. Testing and characterization results are then reported, followed by a discussion of these results. The paper ends with a conclusion summarizing the key findings of this work.

Heat Sink Design

Two commercially available heat sinks were first acquired: one pin-based and one fin-based. The heat sinks that were chosen to fit on top of a microelectronics heat spreader on a 37.5 x 37.5mm substrate typical for CPUs. A combination of design drawing data and actual measurements with calipers were used to model these components in SolidWorks™ [8] and used to create a baseline comparison for the cooling effect between additive and commercial parts for the same nominal design. These designs are shown in Figure 1a and 1b for the commercial pin- and fin-based heat sinks, referred to henceforth as COM Pin and COM Fin.

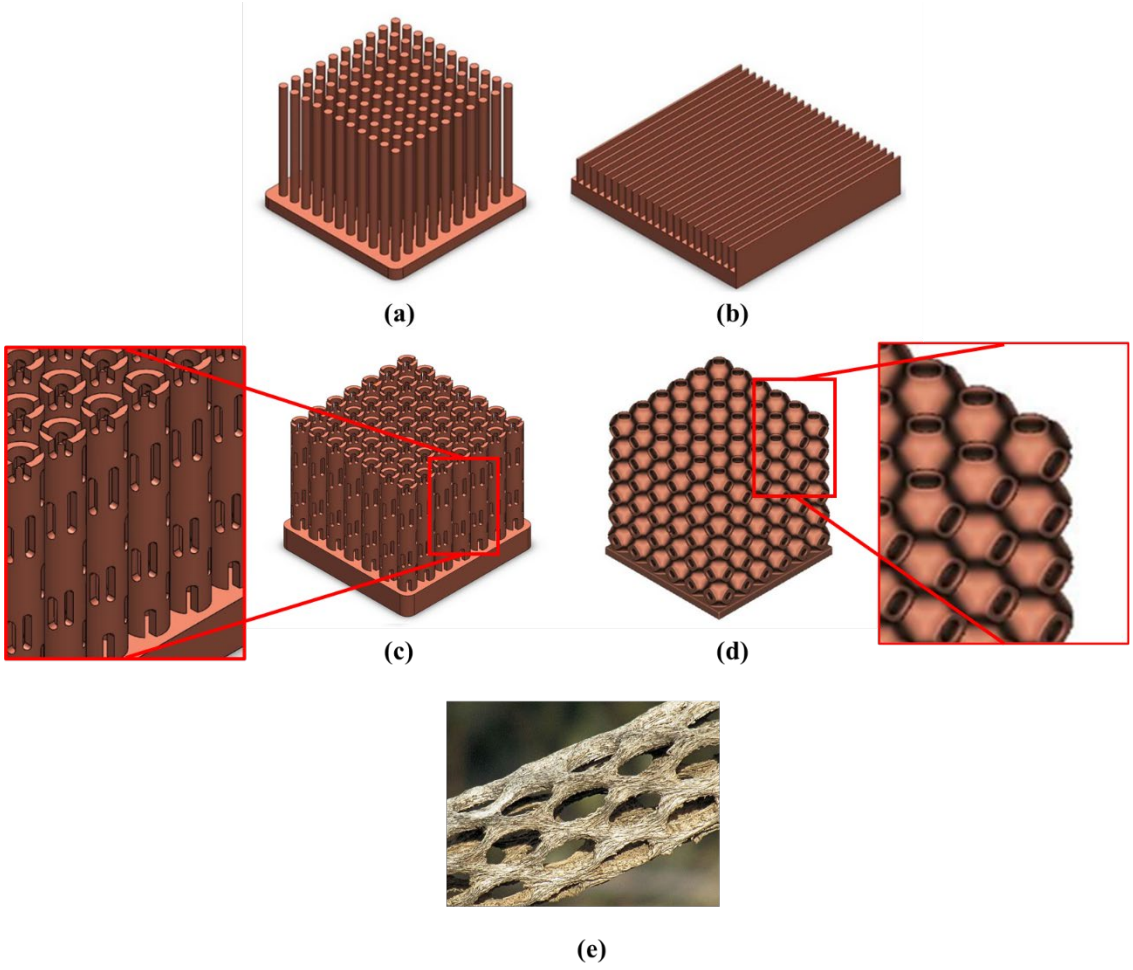

Figure 1. The four different heat sink designs explored in this work: (a) pin, (b) fin, (c) Cholla cactus inspired, (d) Schwarz-P TPMS, and (e) the cholla cactus skeleton that served as inspiration for one of these designs

The second pair of designs followed a bio-inspired approach. The first of these, shown in Figure 1c, was inspired by the skeleton of the cholla cactus, shown in Figure 1e. This particular organism was chosen for its lightweight structural performance [9], and also its ability to survive in extreme climates. In particular, the perforations along the cylindrical structure suggests an ability to enhance convection by enabling access to the interior surface and potentially improving overall heat sink performance, which has been previously shown to improve airflow for both natural and forced convection for similarly shaped structures [10]. For this work, perforations were placed along a spiral path, following the structure of the cholla cactus, also designed in SolidWorks™. The second bio-inspired design leveraged Triply Periodic Minimal Surfaces (TPMS) design which have now been well studied for a range of applications, and while they owe their origins to mathematical formulation, have also been found in several biological structures [11]. TPMS structures are essentially cellular materials, and span a wide range of application domains, and design exploration of this domain has grown significantly with the advancements in additive manufacturing [12], and a bio-inspired design approach is often employed when selecting a particular cellular material for a specific application [13] For this work, the Schwarz-P TPMS structure was selected, based on its high surface area to volume ratio, and the efficient thermal performance of these structures as reported in the literature [14]. These structures were designed in the Platform software developed by nTopology™ [15].

Manufacturing

The 100W Concept Laser MLab LPBF system was used in this work. This machine is considerably lower in maximum power than those typically used in the literature [1], [16], [17], so the first step was to establish a process that could perform at under 100W of laser power. Using the optimal parameters found in other papers working with the CuNi2SiCr alloy, an initial process window was defined for scan speed, hatch spacing, laser power to achieve similar Volumetric Energy Densities (VED) as those reported in the literature. This was used to narrow a set of parameters for further refinement, summarized in Table 1. A total of 16 design points spanning the range of parameters shown in Table 1 were evaluated by building 10mm cube specimens on a 4x4 grid as shown in Figure 2a and 2b. The specific levels for each parameter varied across the range based on preliminary findings not reported here, in order to obtain a wide spread of VED. The cross section of each cube also shows the as printed porosity as seen in Figure 2c, under a microscope. A concern in the development of the process was the risk for oxidation of the copper powder, and the likelihood that this could result in degradation of printed density over time. As a result, the same set of 16 cubes with identical process parameters were fabricated over a four-week period, beginning with virgin powder that immediately went from an unopened container into the MLab dose chamber and was used for fabrication within 4 hours, during which time the machine was inerted with Argon gas. Once the print was completed, the powder was left in the machine for a week at a time (in ambient conditions), and the same build repeated. The 64 specimens obtained were characterized using the Archimedes density method [18] within two days of being printed (including the wire-EDM process to remove the specimens from the build plate), and the results obtained are shown in Figure 3.

Table 1. Range of parameters evaluated in process development for CuNi2SiCr with LPBF

Layer Thickness (mm)	Laser Power (W) Range	Hatch Spacing (mm) Range	Laser Speed (mm/s) Range
0.03	30 – 88	0.1 – 0.17	39 - 200

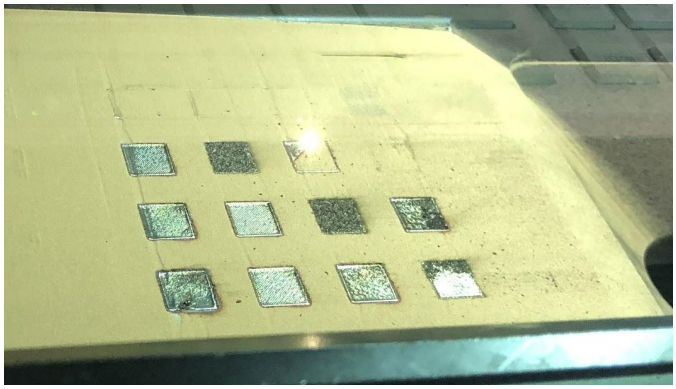

(a)

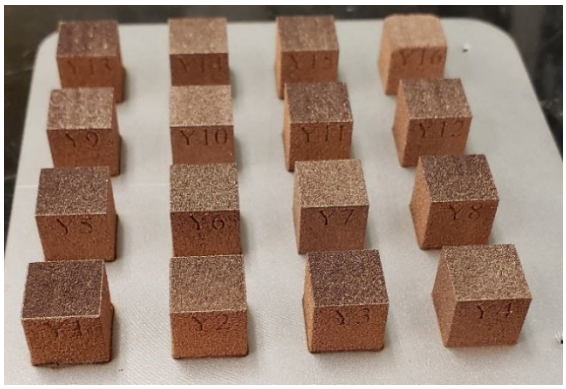

(b)

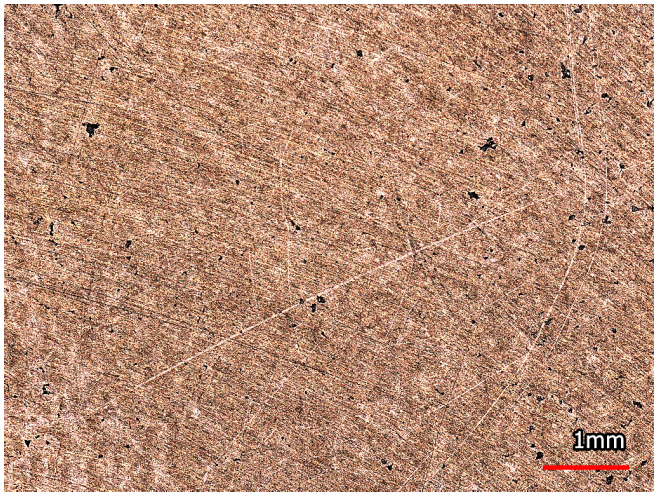

(c)

Figure 2. LPBF of CuNi2SiCr to establish a process for heat sink manufacturing; (a) in-process image of the Concept Laser MLab fabrication process; (b) 10mm cubes of CuNi2SiCr as-printed while still on build platform, awaiting wire-EDM; and (c) cross-section of optimum process selected for heat sink manufacturing

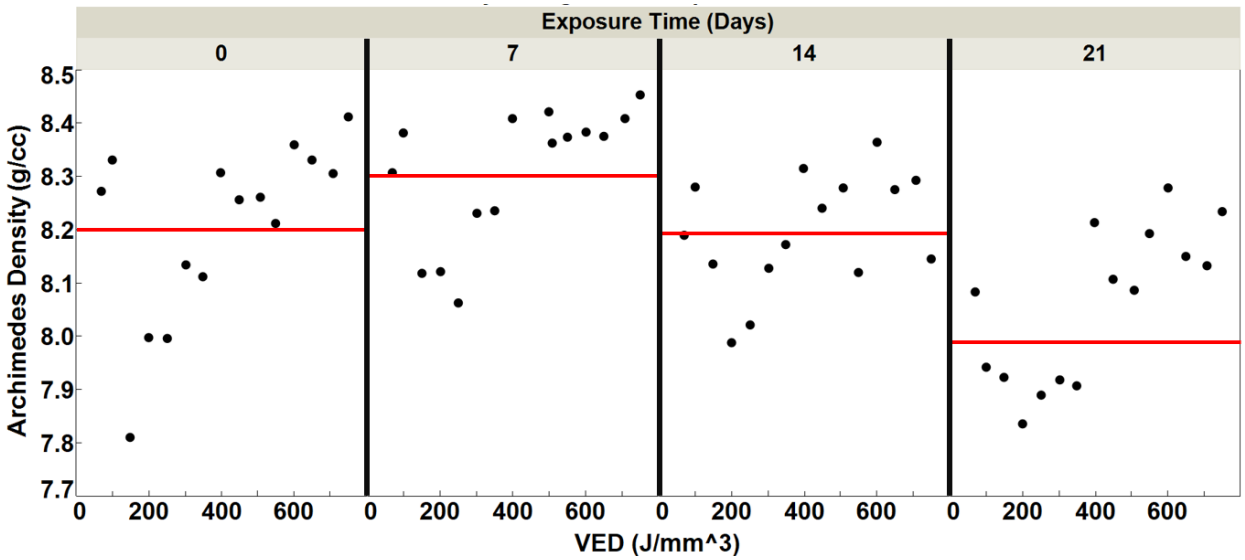

Figure 3. Archimedes density for the 16 cubes as a function of VED and the exposure time, showing no significant changes with time at least for the first 2 weeks of exposure with the red lines indicating the average density.

The first thing of note in Figure 3 is that the density range for the specimens tested spanned approximately 7.8 to 8.5 g/cc, whereas the reported density for this alloy from one supplier's datasheet is 8.85 g/cc [19], indicating that the process developed with the 100W laser has room for improvement. The second thing of note is that the density did not show significant degradation, at least over the first 14 days, with slight reduction observed after 21 days. This data therefore suggests that oxidation risks for CuNi2SiCr, at least in the context of density, are manageable and for this particular study set a 2-week limit on fabricating parts with freshly opened powder.

Based on these findings, an optimum process parameter set was selected as the one that gave the highest average density across all four weeks, which amounted to 94.3% relative density, with the datasheet value [19] used as a baseline. It is important to note that this reported value was not from the same equipment or powder supplier. Nonetheless, this was the highest relative density value attainable within the period of study on the Concept Laser MLab 100W, and a cross-section of one of the samples that employed these parameters is shown in Figure 3c. The relatively slow scan velocity is indicative of the need for high VED for this process.

- Layer thickness: 0.03mm
- Laser power: 85 W
- Scan velocity: 47 mm/s
- Hatch spacing: 0.1 mm
- Continuous scan pattern

In addition to Archimedes density method, two cylinders (25mm tall and 11mm diameter) were fabricated for estimation of thermal conductivity using the hot-disk sensor method [20]. Their bases were polished prior to testing. The resulting thermal conductivity measurement for the LPBF-fabricated CuNi2SiCr specimens was a mere 30 W/mK, substantially less than the 350-390 W/mK reported for commercially pure Copper, and a third as much than that reported by the

datasheet obtained, where the as-printed thermal conductivity was stated to be 90 W/mK, which increased to 190 W/mK after precipitation hardening [19].

Once these parameters were finalized, heat sinks were fabricated with them and are shown collectively in Figures 4a-4f. The AM Fin (Figure 4a) and AM Pin (Figure 4c) heat sinks were manufactured using the same design as the two COM heat sinks (Figures 4b and 4d) for a comparison to isolate the difference in thermal performance between pure copper commercially fabricated heat sinks and the CuNi2SiCr sinks fabricated with LPBF. Following these prints, the Cactus inspired, and Schwarz-P heat sinks were fabricated with LPBF and are shown in Figure 4. Similar to the AM parts, the bio-inspired heat sinks both had 5mm of copper added to the base for base plate removal tolerance. There was a 5mm allowance added to the bottom of the heat sinks so they could be removed from the build plate with a wireEDM without cutting too deep into the heat sink base. The specimens were then ground down to match the cross-section thickness of the COM heat sinks prior to testing.

Heat Sink Characterization and Testing

The first observation of the differences between the COM and AM heat sinks is the surface roughness, with AM heat sinks being significantly rougher, as expected for LPBF, as shown in Figures 5a-5f. To quantify this roughness, regions were selected within the four AM and two COM heat sinks, as shown in the green boxes in Figures 5a-5f, and scanned under the Keyence VR-3200 structured white light scanning microscope [21] using the in-built curved surface correction algorithm to obtain an S_a value. The obtained roughness values from the six heat sinks are given in table 2. While the AM heat sink roughness values are highly dependent on orientation of the scanned region relative to the build platform, they nonetheless are indicative of the differences between commercially fabricated, and as-printed LPBF heat sinks with regard to surface morphology – this difference is very significant for the pin-based heat sinks, but not as significant for the fin-based sinks, since the commercial fin-based sink had a far more striated texture (Figure 5d) compared to the smooth pin texture (Figure 5b). The AM heat sinks were also measured using calipers and all measurements were found to be within 10% of the nominal design, for the commercial and bio-inspired heat sink designs.

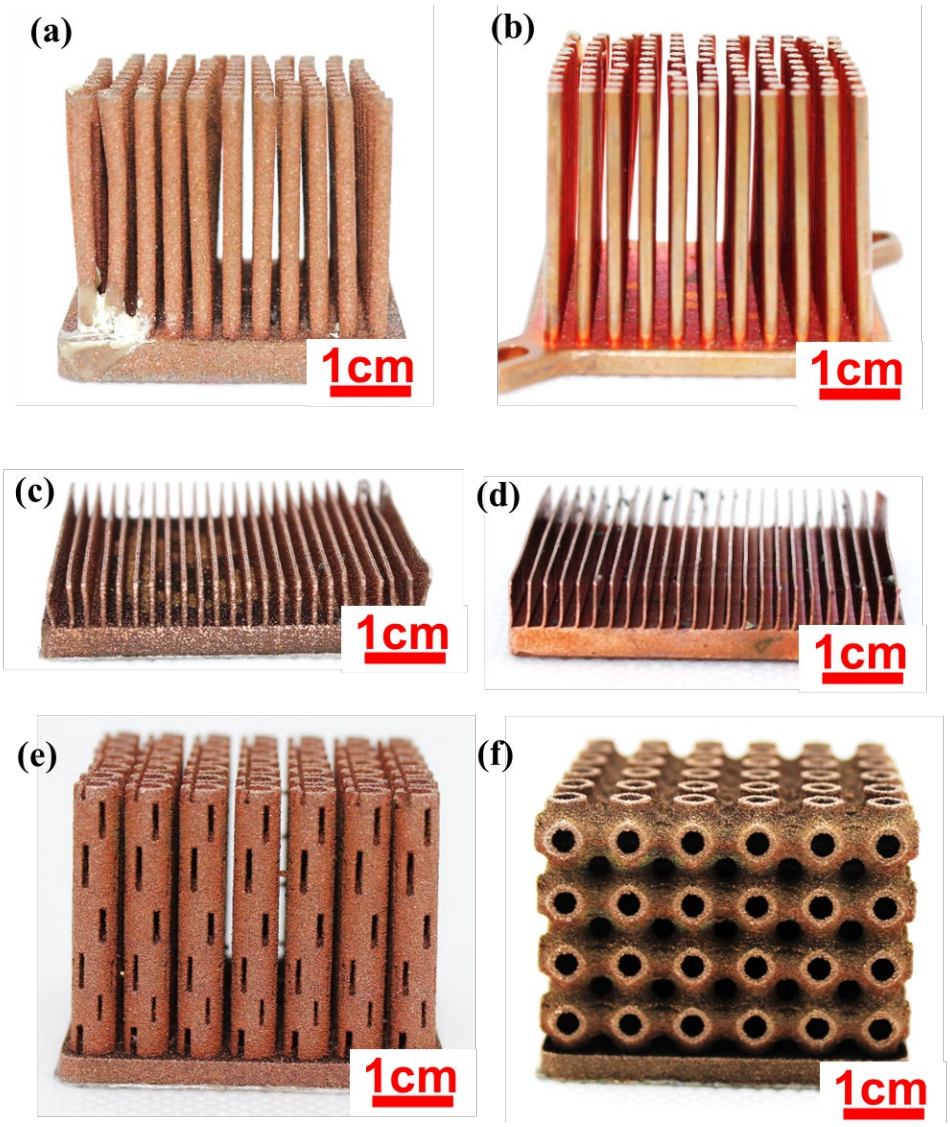

Figure 4. Additive manufactured heat sinks next to commercially available heat sinks: (a) AM Pin, (b) COM Pin, (c) AM Fin, (d) COM Fin, (e) Schwarz-P, (f) cactus inspired

Table 2. Surface roughness (S_a) value comparisons for the AM and COM heat sinks (all in μm)

AM – Pin	COM – Pin	AM – Fin	COM – Fin	Cactus	Schwarz-P
57	9	59	47	78	90

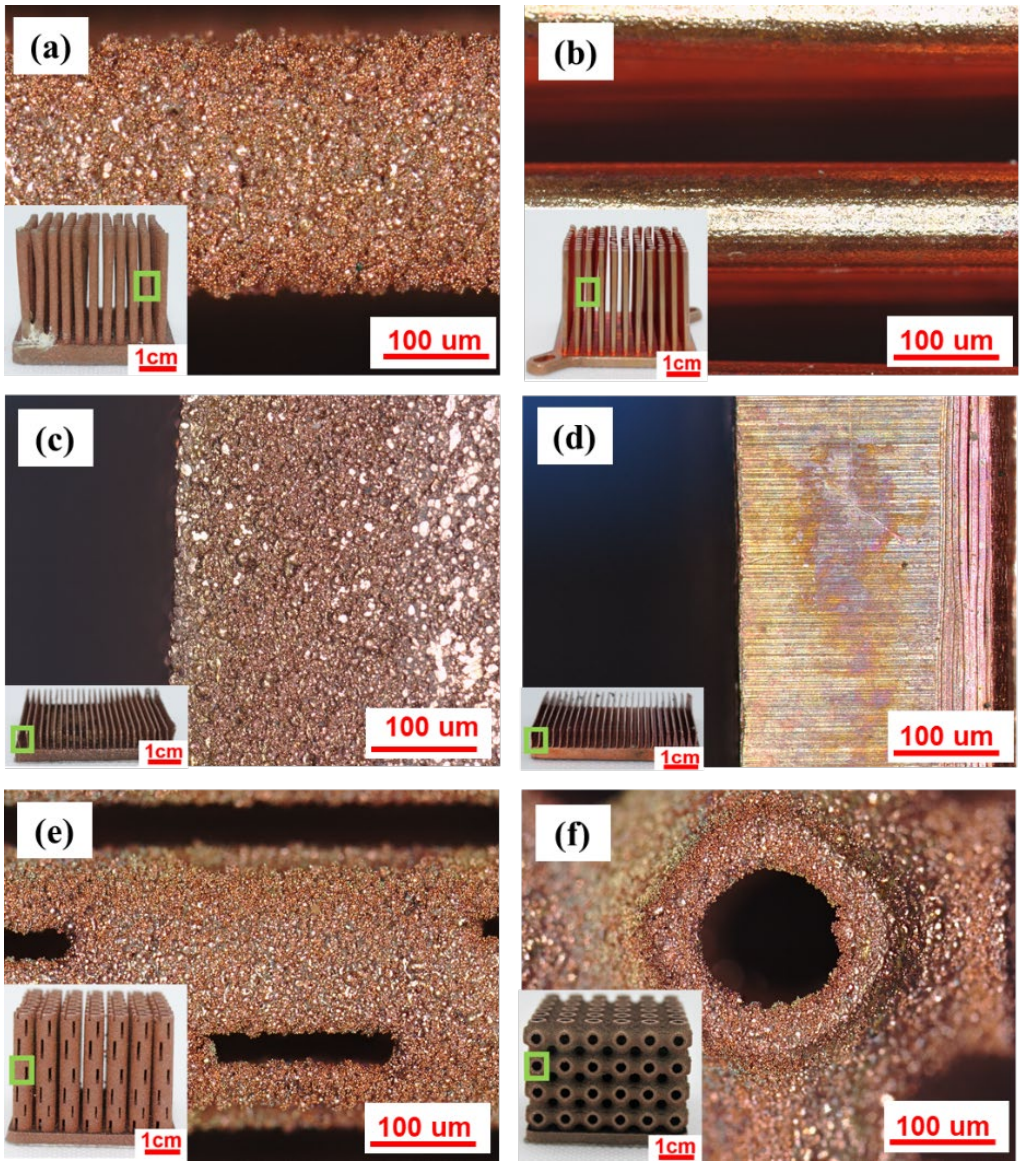

Figure 5. Magnified images of the surface finish of each heat sink and the measurement location used for surface roughness calculation: (a) AM Pin, (b) COM Pin, (c) AM Fin, (d) COM Fin, (e) Schwarz-P, (f) cactus inspired

To estimate the cooling performance of the COM and AM heat sinks, a test setup was built as shown in Figures 6a and 6b, following the setup demonstrated by Constantin et al. [6]. Results obtained with forced convection were highly variable and as a result only natural convection results are reported here. Multiple thermocouples were epoxied to the heat sink and CPU as well as a thermal camera used to detect any hot spot anomalies (none were found and hence not reported here). A hot plate was set to three temperatures for this study: 65, 100 and 150 degrees Celsius. A 37.5mm CPU package was attached to the hot plate using thermal tape. A thermocouple was attached to the surface of the hot plate using Kapton tape to measure the surface temperature of the hot plate during testing. A groove was ground into the CPU heat spreader (as shown in Figure 6c), where a thermocouple was epoxied, and the surface was then sanded smooth. The cooling

effect was defined as the temperature of the CPU thermocouple with and without a heat sink on top of it, after allowing for stabilization of the temperature reading, which took a maximum of 15 seconds (consistent with [10]), which was then set as the standard wait time before recording a measurement. The other thermocouple measurements were used for reference and comparison purposes but not reported here. These measurements were made at three different temperatures – three measurements were made at each condition to obtain an average.

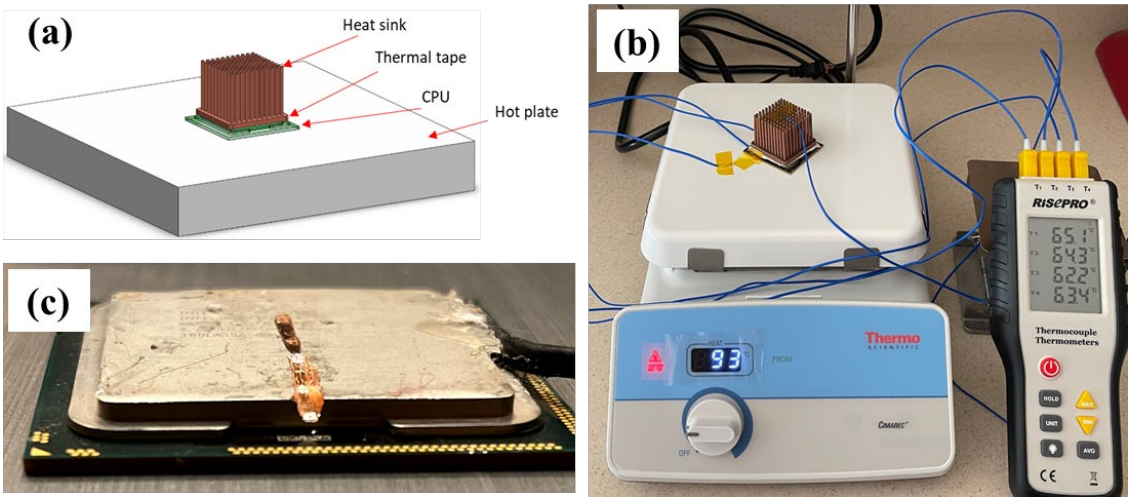

Figure 6. Test setup for measuring cooling effect on account of heat sink: (a) CAD model of the experimental setup, (b) actual test setup used, and (c) groove in heat spreader used to mount thermocouple to obtain measurements right under the heat sink

To first assess the differences between AM and COM heat sinks for the same nominal design, the average change in temperature due to the addition of a heat sink relative to no heat sink is plotted in Figure 7a, at each of the three temperatures for the fin and pin heat sinks. The commercial heat sinks had better in comparison to the AM heat sinks, and the COM pin has the best performance (i.e. highest change in temperature). While neither AM heat sink can compete with the best performing COM heat sink, this is to be expected given the ten-fold reduction in thermal conductivity. However, the fact that both AM heat sinks out-perform the worse COM heat sink with lesser sensitivity to the presence of forced convection is suggestive of the fact that the higher surface roughness in AM specimens disrupts the flow of air, resulting in a greater change in temperature.

To assess the differences in design, the COM Pin design was chosen as a representative baseline since it was the design basis for the bounding box envelope of the bio-inspired structures. The data comparing cooling effects for the bio-inspired heat sink designs against the COM and AM pin heat sinks is shown in Figure 7b. At higher temperatures in particular, it is evident that the bio-inspired designs significantly close the gap between the AM-pin and COM-pin – this is a remarkable outcome given the low thermal conductivity of the LPBF CuNi2SiCr used in this work.

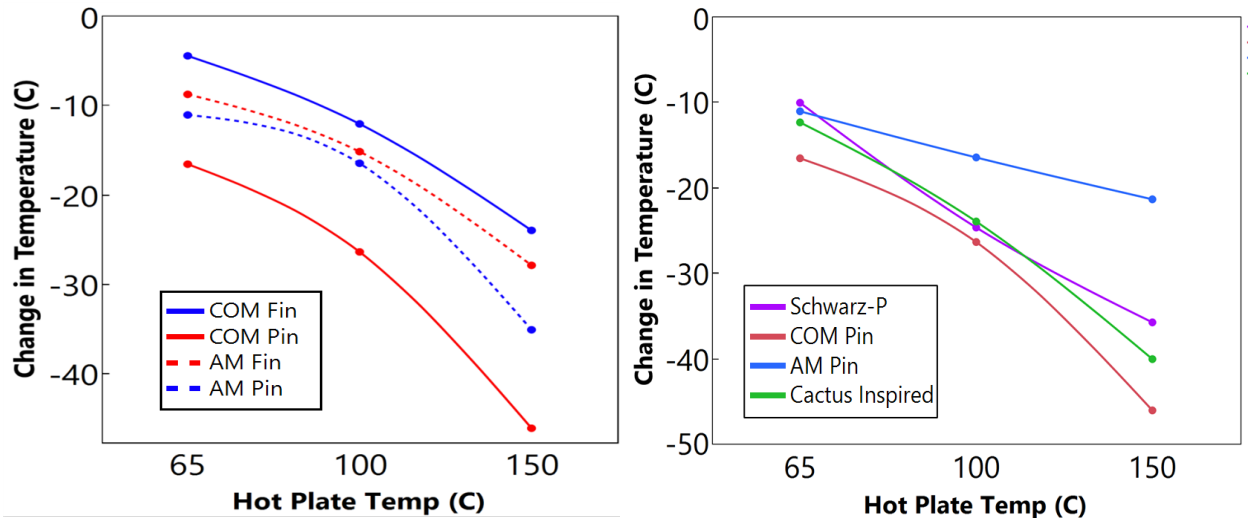

Figure 7. Change in temperature for (a) the four pin- and fin-based designs (b) the bio-inspired heat sinks in comparison to the COM and AM pin heat sinks

Discussion

A key finding of this work is that despite their far lower thermal conductivity, the bio-inspired CuNi2SiCr heat sinks were close in performance to the commercial, pure Copper heat sinks under natural convection conditions. The reasons for this can therefore be attributed to the design and morphology of the bio-inspired heat sinks. An examination of the specific surface area (nominal surface area divided by the mass of the heat sink) for all six heat sinks is shown in Figure 8, clearly indicating the higher values for the bio-inspired designs, which is at least a portion of the explanation for the improved performance. A second contributor to this performance is potentially the higher surface roughness which may play a significant positive role by mitigating against the formation of an insulating boundary layer.

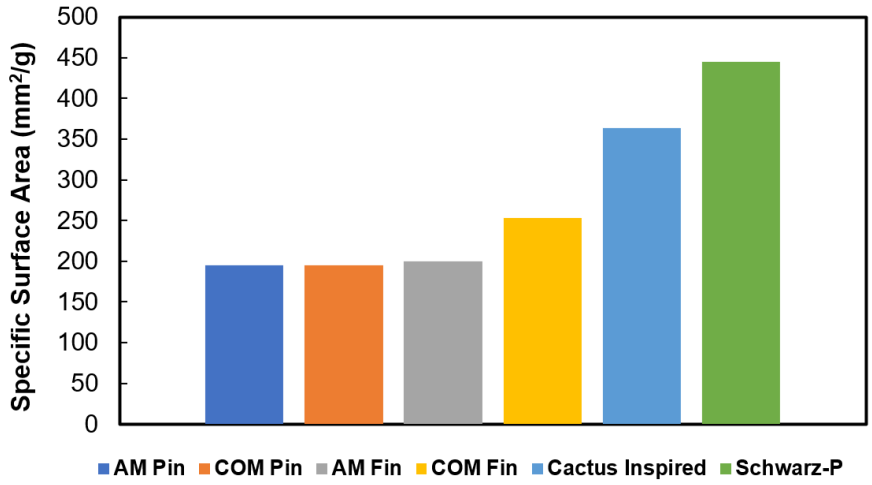

Figure 8. Specific surface area for all six heat sinks used in this work, clearly showing the bio-inspired designs having the highest values

Conclusions

The findings of this work can be summarized in each of the three objectives defined at the outset:

- An LPBF process was developed on a 100W machine for CuNi2SiCr that resulted in 94% dense specimens with thermal conductivity a tenth of commercially pure copper
- LPBF CuNi2SiCr heat sinks when compared to commercial heat sinks made of pure copper showed different performances: additively manufactured fin-based heat sinks outperformed the commercial counterpart, but the pin-based heat sink underperformed, with regard to cooling effect under natural convection conditions
- Finally, despite the very low thermal conductivity, bio-inspired designed heat sinks had comparable performance to the commercial pin-based heat sink, attributable to their higher specific surface area and surface roughness – more work is needed to establish these relationships

This work adds to the body of work demonstrating the benefits of designing for AM to enhance performance. Future work includes replacing CuNi2SiCr with commercially pure copper and examining the effects of heat treatment on thermal performance.

References

[1] T. El-Wardany, Y. She, V. Jagdale, J. K. Garofano, J. Liou, and W. Schmidt, "Challenges in 3D printing of high conductivity copper," in *ASME 2017 International Technical Conference and Exhibition on Packaging and Integration of Electronic and Photonic Microsystems*, 2017, pp. 1–10, doi: 10.1115/ipack2017-74306.

[2] T. Q. Tran *et al.*, "3D printing of highly pure copper," *Metals*, vol. 9, no. 7. MDPI AG, Jul. 01, 2019, doi: 10.3390/met9070756.

[3] C. Silbernagel, L. Gargalis, I. Ashcroft, R. Hague, M. Galea, and P. Dickens, "Electrical resistivity of pure copper processed by medium-powered laser powder bed fusion additive manufacturing for use in electromagnetic applications," *Addit. Manuf.*, vol. 29, Oct. 2019, doi: 10.1016/j.addma.2019.100831.

[4] P. A. Lykov, E. V. Safonov, and A. M. Akhmedianov, "Selective laser melting of copper," in *Materials Science Forum*, 2016, vol. 843, pp. 284–288, doi: 10.4028/www.scientific.net/MSF.843.284.

[5] Y. You *et al.*, "Effect of surface microstructure on the heat dissipation performance of heat sinks used in electronic devices," *Micromachines*, vol. 12, no. 3, pp. 1–12, 2021, doi: 10.3390/mi12030265.

[6] L. Constantin, Z. Wu, N. Li, L. Fan, J. F. Silvain, and Y. F. Lu, "Laser 3D printing of complex copper structures," *Addit. Manuf.*, vol. 35, no. March, p. 101268, 2020, doi: 10.1016/j.addma.2020.101268.

[7] J. Yaple, “Design and Additive Manufacturing of Copper Heat Sinks for Microelectronics Cooling,” Arizona State University (MS Thesis), 2021.

[8] D. Systemes, “Solidworks 2019.” 2019, [Online]. Available: https://www.solidworks.com/.

[9] L. De Vivo *et al.*, “Cholla cactus frames as lightweight and torsionally tough biological materials,” *Acta Biomater.*, vol. 112, pp. 213–224, 2020, doi: 10.1016/j.actbio.2020.04.054.

[10] E. C. Silva, Á. M. Sampaio, and A. J. Pontes, “Evaluation of active heat sinks design under forced convection—effect of geometric and boundary parameters,” *Materials (Basel).*, vol. 14, no. 8, 2021, doi: 10.3390/ma14082041.

[11] L. Han and S. Che, “An Overview of Materials with Triply Periodic Minimal Surfaces and Related Geometry: From Biological Structures to Self-Assembled Systems,” *Adv. Mater.*, vol. 1705708, pp. 1–22, 2018, doi: 10.1002/adma.201705708.

[12] A. du Plessis *et al.*, “Properties and applications of additively manufactured metallic cellular materials: a review,” *Prog. Mater. Sci.*, vol. 125, no. April 2021, p. 100918, 2021, doi: 10.1016/j.pmatsci.2021.100918.

[13] D. Bhate *et al.*, “Classification and Selection of Cellular Materials in Mechanical Design: Engineering and Biomimetic Approaches,” *Designs*, vol. 3, no. 1, p. 19, Mar. 2019, doi: 10.3390/designs3010019.

[14] S. Catchpole-Smith, R. R. J. Sélo, A. W. Davis, I. A. Ashcroft, C. J. Tuck, and A. Clare, “Thermal conductivity of TPMS lattice structures manufactured via laser powder bed fusion,” *Addit. Manuf.*, vol. 30, p. 100846, Dec. 2019, doi: 10.1016/j.addma.2019.100846.

[15] NTopology, “Platform.” New York, 2020.

[16] S. D. Jadhav, S. Dadbakhsh, L. Goossens, J. P. Kruth, J. Van Humbeeck, and K. Vanmeensel, “Influence of selective laser melting process parameters on texture evolution in pure copper,” *J. Mater. Process. Technol.*, vol. 270, pp. 47–58, Aug. 2019, doi: 10.1016/j.jmatprotec.2019.02.022.

[17] C. Zhang, Liu, “Investigation on forming process of copper alloys via SLM,” in *High Value Manufacturing: Advanced Research in Virtual and Rapid Prototyping*, 2013, pp. 285–289.

[18] D. Bruce *et al.*, “A Critical Assessment of the Archimedes Density Method for Thin-wall Specimens in Laser Powder Bed Fusion : Measurement Capability , Process Sensitivity and Property Correlation,” *J. Manuf. Process.*, vol. accepted, 2022.

[19] Zare, “CuNi2SiCr Material Data Sheet,” 2021.

[20] Y. He, “Rapid thermal conductivity measurement with a hot disk sensor: Part 1. Theoretical considerations,” *Thermochim. Acta*, vol. 436, no. 1–2, pp. 122–129, 2005, doi: 10.1016/j.tca.2005.06.026.

[21] “Keyence Corporation of America.” https://www.keyence.com/.